AGU PUBLICATIONS

JGR

Journal of Geophysical Research: Atmospheres

RESEARCH ARTICLE
10.1002/2017JD027904

Key Points:
- Perturbation of the atmosphere by sensible heat from a surface fire is sensitive to vertical canopy structure
- Caution is suggested when extrapolating study findings across forests with different canopy structure

Correspondence to:
M. T. Kiefer,
mtkiefer@msu.edu

Citation:
Kiefer, M. T., Zhong, S., Heilman, W. E., Charney, J. J., & Bian, X. (2018). A numerical study of atmospheric perturbations induced by heat from a wildland fire: Sensitivity to vertical canopy structure and heat source strength. *Journal of Geophysical Research: Atmospheres*, *123*, 2555–2572. https://doi.org/10.1002/2017JD027904

Received 18 OCT 2017
Accepted 8 FEB 2018
Accepted article online 13 FEB 2018
Published online 7 MAR 2018

A Numerical Study of Atmospheric Perturbations Induced by Heat From a Wildland Fire: Sensitivity to Vertical Canopy Structure and Heat Source Strength

Michael T. Kiefer[1], Shiyuan Zhong[1], Warren E. Heilman[2], Joseph J. Charney[2], and Xindi Bian[2]

[1]Department of Geography, Environment, and Spatial Sciences, Michigan State University, East Lansing, MI, USA, [2]U.S. Forest Service, Northern Research Station, Lansing, MI, USA

Abstract An improved understanding of atmospheric perturbations within and above a forest during a wildland fire has relevance to many aspects of wildland fires including fire spread, smoke transport and dispersion, and tree mortality. In this study, the ARPS-CANOPY model, a version of the Advanced Regional Prediction System (ARPS) model with a canopy parameterization, is utilized in a series of idealized numerical experiments to investigate the influence of vertical canopy structure on the atmospheric response to a stationary sensible heat flux at the ground ("fire heat flux"), broadly consistent in magnitude with the sensible heat flux from a low-intensity surface fire. Five vertical canopy structures are combined with five fire heat flux magnitudes to yield a matrix of 25 simulations. Analyses of the fire-heat-flux-perturbed *u* component of the wind, vertical velocity, kinetic energy, and temperature show that the spatial pattern and magnitude of the perturbations are sensitive to vertical canopy structure. Both vertical velocity and kinetic energy exhibit an increasing trend with increasing fire heat flux that is stronger for cases with some amount of overstory vegetation than cases with exclusively understory vegetation. A weaker trend in cases with exclusively understory vegetation indicates a damping of the atmospheric response to the sensible heat from a surface fire when vegetation is most concentrated near the surface. More generally, the results presented in this study suggest that canopy morphology should be considered when applying the results of a fire-atmosphere interaction study conducted in one type of forest to other forests with different canopy structures.

1. Introduction

Wildland fires, by definition, are nonstructure fires that occur in vegetation or natural fuels, and the fuels can include but are not limited to forests. Wildland fires communicate heat to the atmosphere via radiation, convection (i.e., sensible and latent heat flux), and conduction, with sensible and latent heat flux the primary means of perturbing the atmosphere (Jenkins et al., 2001; Kremens et al., 2012). Perturbation of the atmosphere within and above forests by wildland fires has primarily focused on the effects of sensible heat flux from the fire and has been the subject of field experiments (e.g., Clark et al., 1999; Hiers et al., 2009; Heilman et al., 2015) and high-resolution atmospheric modeling studies (e.g., Hoffman et al., 2015; Kiefer et al., 2015, 2016; Pimont et al., 2009, 2011). Numerical modeling studies have found that sensible-heat-induced atmospheric perturbations are sensitive to a number of forest canopy characteristics, including plant area index (PAI), fuel breaks or gaps, and canopy health. For example, Pimont et al. (2009) simulated higher mean wind velocity and greater gust intensity inside a fuel break but reduced variability of wind direction, relative to the surrounding forest, and Kiefer et al. (2015) found that the fireline-normal component of wind and maximum vertical velocity were both lower in magnitude with a horizontally homogeneous sparse canopy than with no canopy, although both variables were largely insensitive to further increases in PAI. As pointed out by Kiefer et al. (2016), an improved understanding of atmospheric perturbations within and above a forest during a wildland fire has relevance to many aspects of wildland fires including fire spread, smoke transport and dispersion, tree mortality, transport of fire embers, and seed dispersal. Note that as in Kiefer et al. (2015, 2016), the term *canopy* is used in this study to describe the entire vegetation layer including, but not limited to, the crown.

An aspect of the forest canopy that has received relatively little attention is the vertical structure of the forest canopy. Vertical canopy structure varies widely in the forested environment, from stands dominated by tree species with dense crowns and tall trunks, such as loblolly (*Pinus taeda*) and maritime (*Pinus pinaster*) pine, to mixed stands with bare deciduous overstory vegetation and evergreen understory vegetation, such as mixed Pitch Pine (*Pinus rigida*) and Scrub Oak (*Quercus ilicifolia*) forests (such as found in parts of the northeastern United States). Furthermore, even in the same forest, seasonal variations in foliage as well as disease and insect outbreaks can alter the vertical canopy structure over various time scales. In a study using the FIRETEC model (Linn & Cunningham, 2005), Hoffman et al. (2015) examined the effect of a multiyear mountain pine beetle outbreak on the mean and turbulent wind fields and fire rate of spread through a forest. In their study, a series of simulations were performed with forest biomass successively removed from the crown and transferred to the surface fuel layer over a 6 year period, to emulate the influence of beetles on tree mortality. Vertical profiles of wind velocity in the undisturbed region upwind of the fire were shown to evolve from a profile typical of forested environments, with weak winds in the lowest two thirds of the canopy and maximum vertical wind shear at and just below canopy top (Finnigan, 2000), to a log wind profile more typical of nonforested environments, with maximum wind shear near the surface. However, Hoffman et al. (2015) did not examine atmospheric variables in the vicinity of the fire, choosing instead to focus on mean fire spread rate and relate that metric to mean wind and turbulence in the undisturbed region upstream of the fire.

In this study, we investigate how the vertical structure of the canopy influences the atmospheric response to a spatially and temporally invariant sensible heat flux at the ground (hereafter, "fire heat flux"), broadly consistent in magnitude with the sensible heat flux from a low-intensity surface fire. We utilize the ARPS-CANOPY model (Kiefer et al., 2013), a version of the Advanced Regional Prediction System (ARPS) model (Xue et al., 2000, 2001) with a canopy parameterization, to systematically examine fire-heat-flux-perturbed atmospheric variables in forests with vertical canopy structure varying from overstory concentrated (i.e., exclusively crown vegetation) to understory concentrated (i.e., exclusively surface vegetation). Also, as a broad parameter space exists with respect to the magnitude of sensible heat fluxes from wildland fires (e.g., Clark et al., 1999; Clements et al., 2007; Heilman et al., 2015), fire heat flux magnitude is varied independently of vertical canopy structure to determine how trends in the magnitude of fire-heat-flux-induced atmospheric perturbations with increasing fire heat flux are affected by vertical canopy structure. Lastly, it is important to note that the fire-atmosphere interactions simulated in this study are one way only; feedbacks from the atmosphere to the fire, as parameterized in two-way interactive models like FIRETEC, are not accounted for here (see section 2.3 for more details).

The remainder of this paper is organized as follows. A description of the model and experiment design are presented in section 2, including a brief overview of the ARPS-CANOPY model (2.1), a description of the model configuration and parameterization (2.2), and a summary of the experiment design (2.3). Results and discussion of the experiments are presented in section 3, beginning with a brief summary of the analysis methodology (3.1) and proceeding in a telescoping manner from two-dimensional horizontal cross sections (3.2), to two-dimensional vertical cross sections (3.3), to one-dimensional profiles (3.4), to summary statistic line plots (3.5). Finally, the paper is concluded in section 4.

2. Model Description and Numerical Experiment Design

2.1. ARPS-CANOPY Overview

The development of ARPS-CANOPY is described in detail in Kiefer et al. (2013), along with validation of the model in an orchard environment; for ARPS-CANOPY validation in a forest setting, see Kiefer et al. (2014). The following is a brief summary of ARPS-CANOPY similar to that presented in Kiefer et al. (2015, 2016)

ARPS-CANOPY is a modified version of the ARPS model in which the effects of vegetation elements (e.g., branches and leaves) on drag, turbulence production/dissipation, radiation transfer, and the surface energy budget are accounted for through modifications to the ARPS model equations. Such changes allow for explicit simulation of airflow through a multiple grid level forest canopy, as opposed to representing the bulk effect of a vegetation canopy on the atmosphere within a single layer, beneath the lowest model grid point (as in, e.g., the standard ARPS model and the Weather Research and Forecasting model, Powers et al., 2017). Although a number of metrics may be used to describe how vegetation is vertically distributed in a column (e.g., the vertical profile of canopy bulk density or the vertical profile of biomass), the vertical profile of plant area density (A_p), defined as the one-sided area of plant material per unit volume, is utilized in ARPS-CANOPY to represent the bulk effects of the canopy on various atmospheric processes (e.g., drag and radiative heating/cooling).

The ARPS model equations were first modified by Dupont and Brunet (2008) to account for the drag force of vegetation elements, via a drag force term added to the momentum equation, and the enhancement of turbulence dissipation in the canopy air space, via a sink term added to the subgrid-scale turbulent kinetic energy (TKE) equation. Note that subgrid-scale turbulence is parameterized in ARPS-CANOPY via a 1.5-order TKE-based turbulence closure (Deardorff, 1980; Moeng, 1984).

Building on the work of Dupont and Brunet (2008), Kiefer et al. (2013) further modified ARPS-CANOPY to allow for simulation of nonneutral canopy flows. Specifically, a term was added to the thermodynamic equation to represent heating (cooling) of the canopy air spaces resulting from the vertical flux convergence (divergence) of net radiation intercepted by the canopy, and the ground radiation budget was modified to account for shading of the ground surface by the overlying vegetation during the day and reduction of outgoing longwave ground radiation at night. To account for the impact of foliage on the radiation budget inside the canopy, a net radiation profile was incorporated that decays downward from canopy top as a function of the cumulative PAI and an empirically determined extinction coefficient (0.6 in this study, as in, e.g., Kiefer et al., 2013; Dupont & Brunet, 2008). Note that calculation of the net radiation budget at canopy top is otherwise identical to the standard ARPS ground radiation budget, except a constant value of albedo appropriate for forested areas is utilized (0.1), and the outgoing longwave component is computed as a function of air temperature at canopy top, rather than skin temperature. Lastly, a production term was added to the subgrid-scale TKE equation to represent turbulence production in the wakes of canopy elements.

While necessitated by the choice of model, the use of A_p serves an additional purpose: since PAI is simply vertically integrated A_p, the overall density of the forest canopy (as measured by PAI) may be fixed, while the vertical distribution of vegetation (as measured by A_p) is varied. It is important to note that ARPS-CANOPY does not resolve the flow around individual trees or the heating/cooling of individual branches or leaves. It is also important to note that aside from the modifications outlined here, ARPS-CANOPY is identical to standard ARPS.

2.2. Model Configuration and Parameterization

In addition to the 1.5-order subgrid-scale turbulence closure scheme referenced in the previous section, the model configuration and parameterization options utilized are as follows. Radiation physics following Chou, (1990, 1992) and Chou and Suarez (1994) are applied outside of the canopy, with the radiation parameterization outlined in section 2.1 applied at points inside the canopy. Fourth-order accurate finite differencing of the advection terms is used in both the vertical and horizontal directions. Coriolis terms are retained in the model equations, but the Coriolis force is computed as a function of central latitude only (arbitrarily specified as 40°N).

Using a model configuration identical to Kiefer et al. (2016), a one-way nesting procedure is utilized with two three-dimensional computational domains. The outer domain consists of 153 × 103 × 78 grid points (including points used only for boundary condition calculations), with 50 m horizontal grid spacing and a periodic boundary condition at the lateral boundaries. The inner domain, centered within the outer domain, consists of 99×51×78 grid points, with 10 m horizontal grid spacing and external lateral boundary conditions (i.e., defined by interpolating variables from the outer-domain grid to the boundaries of the inner domain). Vertical grid spacing of 2 m is utilized in both domains, up to a height of 84 m, above which vertical stretching is applied; this vertical grid structure allows for 9 grid points at or below the canopy crown [canopy height (h) is 18 m]. The top of both model domains is at 3 km, with a rigid lid upper boundary condition and a Rayleigh damping layer in the uppermost 1 km to prevent reflection of waves from the upper boundary.

The outer-domain simulation is initialized at noon local time and run for a total of 4 h, with a uniform, steady net radiation flux of 520 W m^{-2} applied at the canopy top to represent daytime heating typical of 40°N latitude in early spring. The outer-domain simulation is run with a uniform canopy (see section 2.3) and no-fire heat flux and is initialized with a base state sounding consisting of uniform wind speed (2.5 m s^{-1}, westerly) from the surface to domain top and neutral static stability below $z = 1$ km [stable stratification ($N = 0.013$ s^{-1}) above]. At initialization, the ground surface temperature is 290 K and the soil is in equilibrium with the overlying atmosphere. To promote the development of 3-D turbulent structures following a horizontally homogeneous initialization, a random perturbation of magnitude 1 K is applied to the potential temperature field at the initial time (at all model levels). After approximately 3 h a quasi-horizontally homogeneous and quasi-stationary planetary boundary layer develops, and the inner-domain simulation is initialized at the end of hour three. The inner-domain simulation is run for 1 h, with uniform net radiation flux applied as in the outer-domain

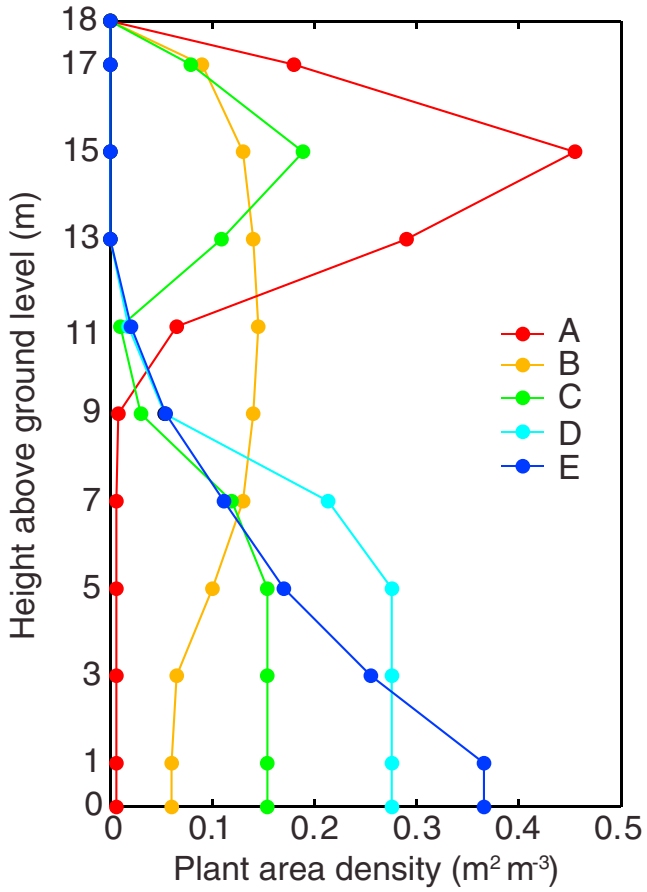

Figure 1. Vertical profiles of plant area density (A_p) for the five vertical canopy structures explored in this study; note that for all canopy profiles, plant area index = 2 and h = 18 m. See the main text for a description of the relationship of each profile to observed forest stands.

simulation, with one-way lateral boundary conditions applied every time step but updated every 5 min (that is, output files from the outer-domain simulation are read in every 5 min).

2.3. Experiment Design

A total of 25 inner-domain simulations is performed in this study, with five vertical canopy structures, as represented by A_p profiles, and five fire heat flux magnitudes. Note that for each A_p profile, the outer-domain simulation (without fire heat flux) and corresponding inner-domain simulations (with and without fire heat flux) use the same profile, yielding a grand total of 30 simulations: 5 outer-domain simulations and 25 inner-domain simulations. To represent the range of vertical canopy structures discussed in section 1, five A_p profiles are utilized with letter designations assigned as shown in Figure 1, ordered from most overstory concentrated (A) to most understory concentrated (E). Of the five profiles examined in this study, three were originally presented in Dupont and Brunet (2008) (profiles A, B, and C, corresponding to their cases 2, 1, and 3, respectively). Profile A features a dense crown layer and sparse trunk space and is broadly representative of a maritime or loblolly pine stand, whereas the more uniformly distributed profile B is based on a deciduous forest stand in Ontario, Canada (Shaw et al., 1988); profile C is a variation on profile A in which two distinct crown and understory vegetation layers exist. In addition to profiles A–C, two additional profiles (D and E) are included here to consider forests in which vegetation is concentrated near the ground, such as wintertime deciduous forests with evergreen understory vegetation. Profile D is a variation on profile C in which the crown vegetation is removed and redistributed to the understory, but the overall shape of the understory profile is retained. Finally, profile E is one in which vegetation density decreases exponentially away from the surface and is based on Light Detection and Ranging (LiDAR)-derived profiles of A_p obtained in a mixed Pitch Pine-Scrub Oak forest stand in New Jersey (Kiefer et al., 2014). Note that for all five canopy profiles, PAI = 2 and h = 18 m.

Complementing the five vertical canopy structures, five fire heat flux magnitudes are examined by varying sensible heat flux within a 50 m wide strip (hereafter, "fireline") between 0 kW m^{-2} (hereafter, "no-fire") and 100 kW m^{-2}, with a 25 kW m^{-2} interval between cases. Values between 25 and 100 kW m^{-2} fall within the envelope of 1 min mean sensible heat fluxes reported during field studies of low-intensity fires (8–155 kW m^{-2} (e.g., Clements et al., 2007; Hiers et al., 2009; Heilman et al., 2015). Surface heat fluxes in this study are restricted to a range representing low-intensity fires due to uncertainty regarding the suitability of some of the underlying assumptions in the ARPS model for higher-intensity fire simulations (e.g., potential temperature perturbations must be small relative to the base state). We include this cautionary statement about the small perturbation limitation of the modeling framework out of an abundance of caution. It is important to keep in mind that ARPS/ARPS-CANOPY have been successfully applied to studies of the fire-heat-flux-perturbed atmosphere (e.g., Dahl et al., 2015; Kiefer et al., 2009, 2014, 2016), and other models with more restrictive assumptions than ARPS/ARPS-CANOPY have been utilized extensively in studying fire-atmosphere interactions (e.g., the Clark coupled fire-atmosphere model, with the anelastic approximation, Clark et al., 2004). Furthermore, it is worth noting that ARPS-CANOPY was developed primarily for low-intensity fire applications, wherein transport and dispersion of smoke are especially sensitive to local vegetation. However, although a heat source has been implemented in ARPS-CANOPY in this and previous studies (e.g., Kiefer et al., 2016), ARPS-CANOPY was not exclusively designed for fire applications. As an atmospheric model with a canopy parameterization, it has also been applied in nonfire environments (e.g., Kiefer et al., 2013; Kiefer & Zhong, 2015).

The fireline is positioned 3.2 km downstream of the western boundary and is applied following a 30 min spin-up period after the inner-domain initialization. The fireline extends the length of the domain in the y direction (500 m), and the fire heat flux is applied for a total of 30 min. In order to avoid possible unphysical atmospheric phenomena associated with a single-grid-point-wide fireline, the heat flux is laterally distributed across the fireline in a step pattern, with 85% of the total heat flux (21.25 kW m^{-2}) applied at the center grid point, and the fire heat flux in the flanking cells stepping down to zero three cells away. Lastly, note that given the 2.5 m s^{-1} westerly base state wind, the fireline is oriented perpendicular to the ambient wind.

Before proceeding, it is worthwhile to discuss some possible limitations of the idealized modeling framework used in this study. As pointed out by Kiefer et al. (2016), the heat source from the fire is represented in ARPS-CANOPY as a static line of enhanced surface sensible heat flux that is independent of temporal and spatial variability of the atmosphere, as well as the overlying forest canopy. The complex interactions between fire, fuels, and atmosphere represented in coupled fire-atmosphere models like FIRETEC are not accounted for in ARPS-CANOPY; the only interaction represented in ARPS-CANOPY is the perturbation of the atmosphere due to the sensible heat flux from the fire. Also, it is important to keep in mind that the horizontally homogeneous forest utilized in this study is an idealization of real-world forests in which different species of trees, and trees in different stages of development, coexist in a complex mosaic of tree stands, isolated trees, and open spaces. Although the results of this idealized study are expected to have applicability to real-world forests, the complication of flows due to the horizontal heterogeneity of a real-world forest will likely modulate the relationships studied herein. Note that temporally and spatially invariant sensible heat fluxes and A_p profiles are representative of an idealized scenario in which a slow-moving low-intensity fire exclusively consumes dead fuels in a horizontally homogeneous fuel bed, leaving live surface and crown fuels intact. Thus, while appreciating the advantages of an idealized modeling framework (e.g., reducing complexity and uncertainty related to fire spread routines), the reader is advised to keep the limitations of such a framework in mind when interpreting the results of this study.

Here and throughout the remainder of this manuscript, a case-naming convention is utilized wherein the A_p profile and fire heat flux magnitude combination are explicitly indicated in the case name; for example, case A0 refers to profile A and 0 kW m^{-2} fire heat flux (i.e., no fire), and case E75 refers to profile E and 75 kW m^{-2} fire heat flux.

3. Results and Discussion

3.1. Analysis Methodology

Five variables are examined in this study: horizontal wind speed (S), u component of the wind (U), vertical velocity (W), kinetic energy (E), and temperature (T); the v component of the wind (V) is used in intermediate processing but is not explicitly analyzed in this study. Following Kiefer et al. (2016), perturbation wind

components are computed by subtracting 30 min mean quantities from the no-fire simulation from the instantaneous time series output every second,

$$u'_F = u_F - \overline{U}_{NF} \qquad v'_F = v_F - \overline{V}_{NF} \qquad w'_F = w_F - \overline{W}_{NF} \tag{1}$$

where the prime denotes perturbations, F and NF subscripts refer to simulations with and without fire heat flux, and the bar denotes a time average. Note that these perturbations should not be confused with turbulent fluctuations, which are computed by subtracting the time average in the presence of fire heat flux from the instantaneous time series,

$$u''_F = u_F - \overline{U}_F \qquad v''_F = v_F - \overline{V}_F \qquad w''_F = w_F - \overline{W}_F \tag{2}$$

where the double prime denotes turbulent fluctuations. Note that turbulence associated with the ambient wind field also contributes to the turbulent fluctuations that occur in the presence of the fire heat flux. We define perturbations as in equation (1) because we are interested in examining the total influence of the fire heat flux on the atmospheric variables. Solving for the instantaneous components in equation (2) and substituting them into equation (1), it can be shown that

$$u'_F = u''_F + \overline{U}_F - \overline{U}_{NF} \qquad v'_F = v''_F + \overline{V}_F - \overline{V}_{NF} \qquad w'_F = w''_F + \overline{W}_F - \overline{W}_{NF} \tag{3}$$

Thus, the perturbation as it is defined here is the sum of a turbulent fluctuation part (e.g., u''_F) and a mean anomaly part (e.g., $\overline{U}_F - \overline{U}_{NF}$). Examples of mean anomalies include the stationary updraft (stationary relative to turbulent fluctuations) and the persistent heated zone above the fireline, both induced by the strong heat release into the atmosphere. The mean anomaly is the primary metric analyzed in sections 3.3 and 3.4.

The resolved E, computed as $\frac{1}{2}\left(u'^2_F + v'^2_F + w'^2_F\right)$, is therefore a complete measure of the impact of the sensible heat released from the fire on the kinetic energy of the resolved flow. The resolved E is subsequently combined with the subgrid-scale TKE (computed internally in ARPS-CANOPY; section 2.1), to yield total E (hereafter, the "total" is omitted). Note that E as it is computed in this study is not equivalent to TKE since the perturbation wind components used to compute the resolved E contain both turbulent fluctuations and mean anomalies. Also note that although this study of atmospheric perturbations above wildland fires has relevance to multiple aspects of such fires (e.g., fire behavior and tree mortality), our purpose in presenting E is to characterize changes to both turbulent mixing and mean transport of heat, moisture, and pollutants (e.g., particulate matter with diameters of 2.5 μm or less, $PM_{2.5}$) due to the sensible heat released from the fire.

Finally, all quantities are averaged over the 30 min period during which the fire heat flux is applied, and with the exception of S, along the entire y axis as well, excluding the north and south lateral boundary points. Temporal and spatiotemporal averaging are expressed as $\overline{\Phi}_t$ and $\overline{\Phi}_{yt}$, respectively, where Φ is the variable name and "t" and "y" refer to averaging in time and the y direction, respectively. A telescoping approach is utilized in which the aforementioned variables are examined in near-surface horizontal cross sections first (3.2), west-east oriented vertical cross sections second (3.3), vertical profiles third (3.4), and summary box-and-whisker plots last (3.5).

3.2. Horizontal Cross Sections

In this section, horizontal cross sections of near-surface flow across the fireline are examined in order to both assess the impact of vertical canopy structure and fire heat flux magnitude on atmospheric flows near the surface and provide some context for subsequent analyses. Figure 2 contains a 5 × 5 matrix of horizontal cross sections of $\overline{S}_t$ (shaded), $\overline{W}_t$ (contoured), and $\overline{U}_t$, $\overline{V}_t$ streamlines at 1 m above ground level (AGL) (five A_p profiles; five fire heat flux magnitudes). It is important to keep in mind that Figure 2 shows the mean flow in each simulation, not the mean anomaly, as is examined in subsequent figures. First, note that in the absence of fire heat flux, $\overline{S}_t$ is less than 1 m s^{-1} and exhibits a lack of sensitivity to vertical canopy structure (Figure 2, fifth row). However, the patterns of converging and diverging flow seen in the streamline fields in each panel, evidence of turbulent eddies in the convective planetary boundary layer, do differ from case to case. Lastly, note that $\overline{W}_t$ at 1 m AGL is below the minimum contour threshold (1 cm s^{-1}). The weak and variable near-surface wind field shown in the no-fire row of Figure 2 is typical of wind fields observed at the bottom of forest canopies (Finnigan, 2000; Raupach & Thom, 1981).

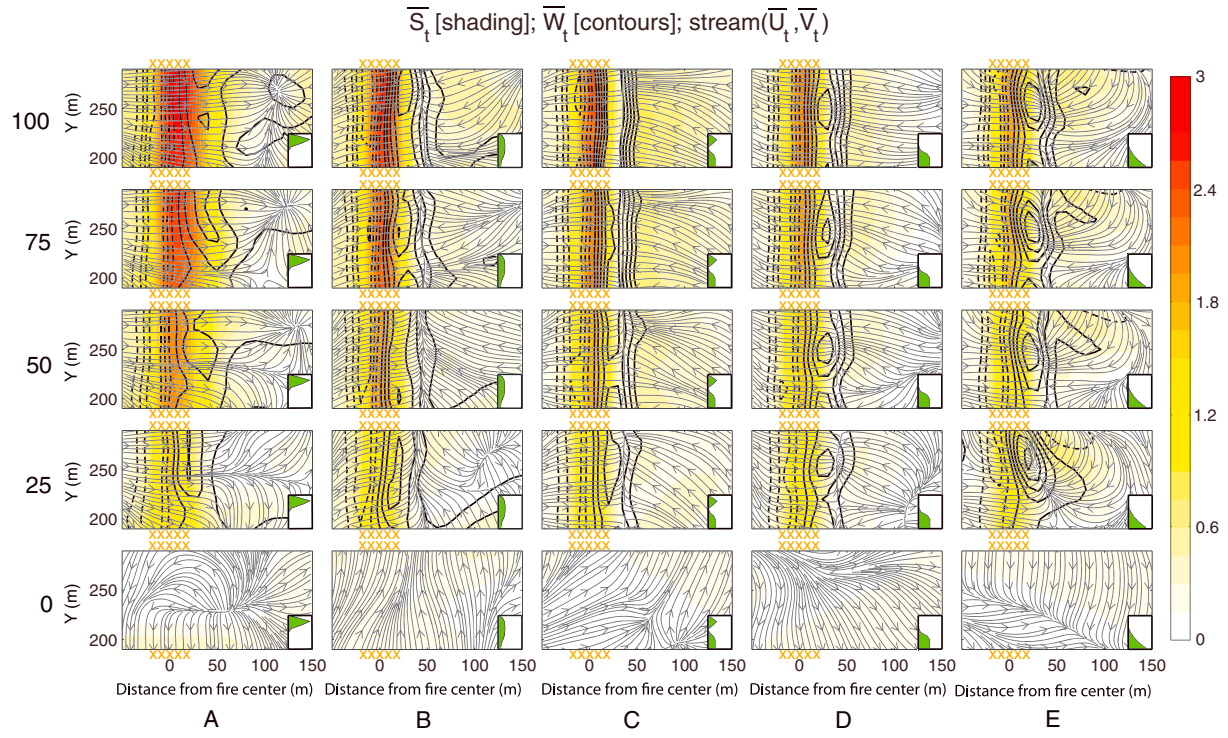

Figure 2. Horizontal cross sections of temporally averaged S ($\overline{S}_t$; m s^{-1}; shaded), W ($\overline{W}_t$; cm s^{-1}; < 0: dashed lines, > 0: solid lines), and horizontal streamlines ($\overline{U}_t$, $\overline{V}_t$), at 1 m above ground level. Panels are arranged in a 5 × 5 matrix with vertical canopy structure varying between panels along the x axis (canopy profiles A–E) and fire heat flux magnitude varying between panels along the y axis (units of kW m^{-2}). Note that a 0.15 m s^{-1} interval is used for $\overline{S}_t$, and a 1 cm s^{-1} interval is used for $\overline{W}_t$. The location of the fireline is denoted above and below each panel with orange cross symbols, and inset panels depict vertical profiles of A_p for each case (Figure 1). Note that only a subset of the domain is displayed in each panel (in the x direction, 50 m upstream to 150 m downstream of the fireline center, and in the y direction, 50 m on either side of the center of the y domain).

Proceeding to the 25 kW m^{-2} fire heat flux row in Figure 2, several points merit discussion. First, a stripe of stronger $\overline{S}_t$ is present above the fireline, with $\overline{S}_t$ approximately 1 m s^{-1} stronger inside the stripe than outside. Second, a $\overline{W}_t$ couplet is evident, approximately centered on the $\overline{S}_t$ stripe, with negative (positive) $\overline{W}_t$ to the left (right) of the fireline. Taken together with the pattern of stronger $\overline{S}_t$ above the fireline, a quasi-two-dimensional counterclockwise circulation is depicted. Third, a semblance of a convergence zone immediately downwind of the fireline is present for canopy profiles B–E; however, the $\overline{U}_t$, $\overline{V}_t$ streamlines depict a wind field only slightly less disorganized than the no-fire row. For canopy profile A, divergent flow is present downstream of the fireline.

As fire heat flux magnitude is increased from 25 to 100 kW m^{-2} (Figure 2, first to fourth rows), $\overline{S}_t$ within the aforementioned stripe doubles from 1–1.5 m s^{-1} to 2–3 m s^{-1}, with $\overline{S}_t$ largest in case A100. The convergent flow, consisting of westerly flow to the left of the fireline and easterly flow to the right, also becomes better defined as fire heat flux is increased. The convergence zone is located near the right edge of the fireline in each of the cases, with the exception of canopy profile A, wherein the convergence zone is displaced about 100 m east of the fireline edge. Although the underlying reason for this displacement is unclear and merits further analysis, the noticeably broader updraft in cases with canopy profile A versus other canopy profiles may be related to this displacement; upward motion above the surface extends well east of the fireline in cases with canopy profile A, as discussed in section 3.3. Changes to $\overline{W}_t$ with increasing fire heat flux appear more subtle, although with the exception of canopy profile E, $\overline{W}_t$ exhibits a steady increase in magnitude in each of the cases. Recalling that $\overline{W}_t$ is analyzed here at 1 m AGL, where vertical motions are understandably weak, further discussion of vertical motion is deferred until vertical cross sections of $\overline{W}_{yt}$ are presented in section 3.3.

3.3. Vertical Cross Sections

The analysis of vertical cross sections begins with $\overline{U}_{yt}$ (Figure 3). Figure 3 contains a 5 × 5 matrix of vertical cross sections (five A_p profiles; five fire heat flux magnitudes) with values for a particular case indicated with black contours and the difference between the mean for that case and the mean for the no-fire case (i.e., the

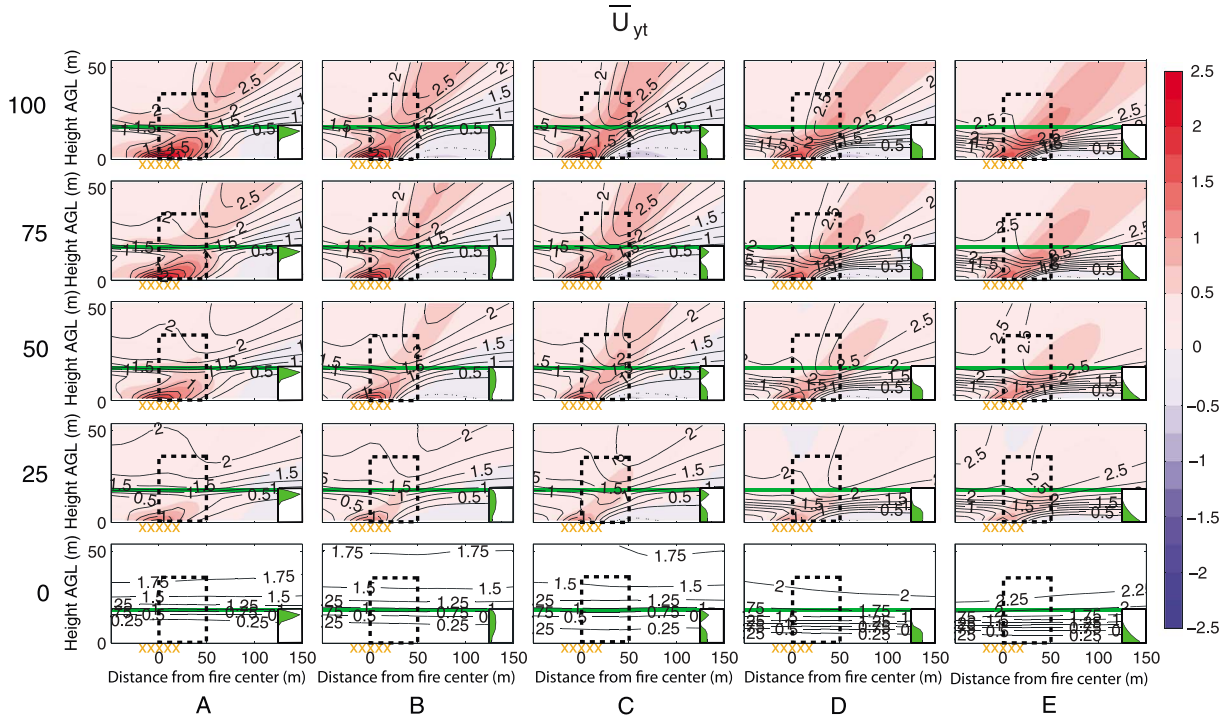

Figure 3. Vertical cross sections of spatiotemporally averaged U ($\overline{U}_{yt}$; m s^{-1}), arranged in a 5 × 5 matrix with vertical canopy structure varying between panels along the x axis (canopy profiles A–E) and fire heat flux magnitude varying between panels along the y axis (units of kW m^{-2}). In each panel, contours depict the values for that particular case, and the shading depicts the difference in values between that case and the corresponding no-fire case, that is, the mean anomaly (0.25 m s^{-1} interval for both contours and shading). The location of the fireline is denoted below each panel with orange cross symbols, the top of the forest canopy is indicated with a solid green line, and inset panels depict vertical profiles of A_p for each case (Figure 1). The averaging zone used to generate the vertical profiles in Figures 7 and 8 is indicated in each panel with a dashed black line. Note that only a subset of the domain is displayed in each panel (50 m upstream to 150 m downstream of the fireline center).

mean anomaly, $\overline{U}_F - \overline{U}_{NF}$) indicated with shading (blue: value smaller than no-fire case; red: value greater than no-fire case). Consider first the influence of vertical canopy structure on $\overline{U}_{yt}$ in the absence of fire heat flux (Figure 3, fifth row). Consistent with the 1 m AGL horizontal cross sections in Figure 2, Figure 3 shows that weak flow less than 0.25 m s^{-1} in magnitude is present near the surface for all vertical canopy structures. Note that although a layer of maximum vertical wind shear is present in all five cases, both the height of the shear layer above the ground and the strength of the shear are sensitive to the canopy profile. Profiles A–C yield shear layers centered near canopy top, with stronger wind shear for overstory-concentrated profile A and weaker wind shear for intermediate profiles B and C; understory-concentrated profiles D and E yield shear layers located approximately midcanopy, with profiles D and E yielding the overall strongest wind shear of the five profiles.

Next, consider the influence of the 25 kW m^{-2} fire heat flux on $\overline{U}_{yt}$ by comparing the bottom two rows of the matrix; as differences may be difficult to discern when comparing contours between panels, focusing on the shaded mean anomaly is recommended. Consistent with the analysis of $\overline{S}_t$ in Figure 2, a positive $\overline{U}_{yt}$ mean anomaly develops immediately above the fireline, a manifestation of westerly inflow into a buoyancy-induced updraft (discussed next in the context of $\overline{W}_{yt}$), and a negative $\overline{U}_{yt}$ mean anomaly develops downstream of the fireline, a manifestation of easterly inflow into the updraft; note also that this pattern exists regardless of canopy profile. Although the positive $\overline{U}_{yt}$ mean anomaly is larger for overstory-concentrated canopies than understory-concentrated canopies, the primary influence of the vertical canopy structure on the $\overline{U}_{yt}$ mean anomaly field is seen in the vertical depth of the negative mean anomaly. The two cases with understory-concentrated vegetation (cases D25 and E25) have shallow negative mean anomaly layers restricted to the lowest few meters of the canopy, whereas the other cases (A25, B25, and C25) exhibit deeper negative mean anomaly layers extending through the canopy into the atmosphere above. Note that the depth of the negative mean anomaly layer is roughly proportional to the height AGL of the layer of maximum background vertical wind shear (compare the depth of the blue shading in the 25 kW m^{-2} row to the height AGL of

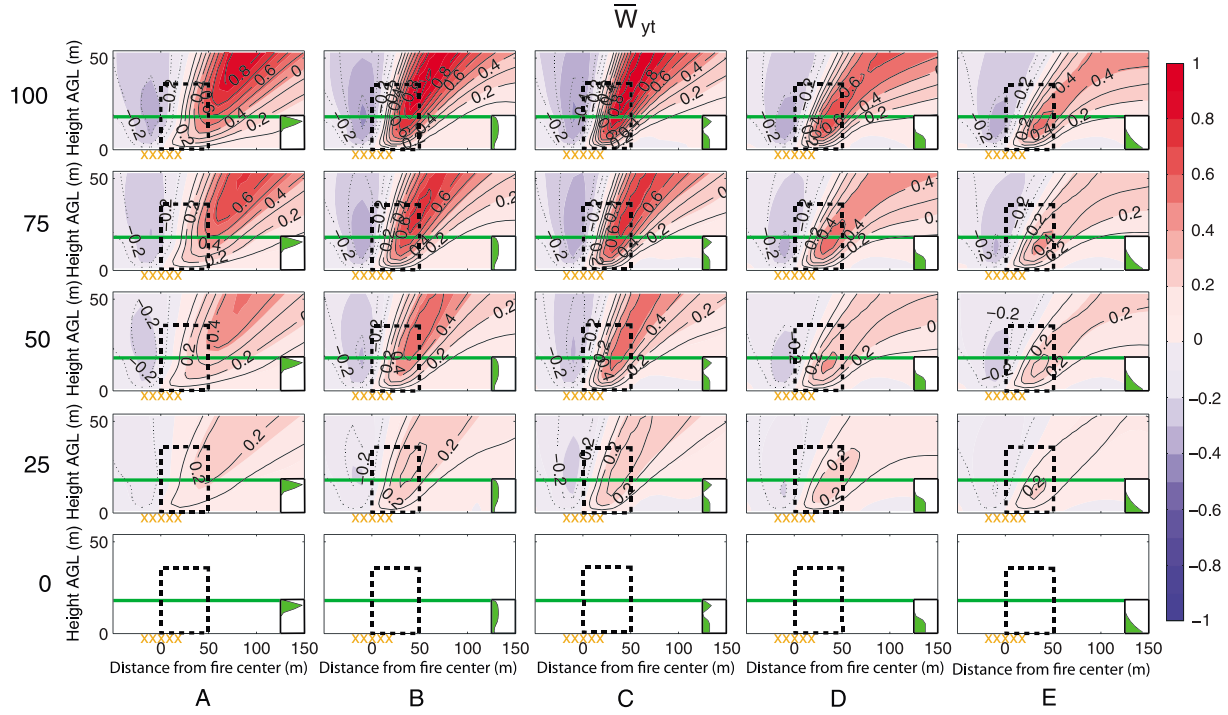

Figure 4. Same as Figure 3 but for W ($\overline{W}_{yt}$; m s^{-1}); interval is 0.1 m s^{-1} for contours and shading.

the more densely packed contours in the bottom row), and in turn approximately proportional to the height AGL of the maximum A_p (Figure 1). These simulations indicate that the presence of vegetation at the bottom of the forest canopy limits the vertical depth of the easterly inflow. Lastly, note that although the mean anomaly spatial pattern is largely insensitive to increases in fire heat flux magnitude (compare the first to fourth rows), the mean anomaly magnitude is not. Mean anomaly magnitude consistently increases with increasing fire heat flux magnitude; the influence of vertical canopy structure on this trend is further addressed in section 3.5.

Proceeding to $\overline{W}_{yt}$ (Figure 4), the absence of contours in the no-fire panels (indicative of values smaller than the 0.1 m s^{-1} contour interval) necessitates comparison of the first to fourth rows only. First, note that introduction of the 25 kW m^{-2} fire heat flux yields a $\overline{W}_{yt}$ mean anomaly pattern broadly similar for all five vertical canopy structures. A mean anomaly couplet is evident in each column of Figure 4, as first seen in Figure 2, consisting of an upright downdraft with a base located near the upstream edge of the fireline and a forward-tilted updraft with a base located near the downstream edge of the fireline. Despite the broadly similar pattern, sensitivity of the mean anomaly pattern to vertical canopy structure is evident. As the canopy structure evolves from most overstory concentrated (case A25) to most understory concentrated (case E25), the updraft and downdraft cores descend from above to below canopy top, while becoming weaker and more concentrated. Note that the height AGL of the $\overline{W}_{yt}$ cores is correlated with the depth of the easterly inflow (cf. Figures 3 and 4), with the inflow and vertical motion fields related via mass continuity. Furthermore, note that the width of the updraft is sensitive to vertical canopy structure, with profile A yielding notably broader updrafts than profiles B–E; the horizontal scale of the downdraft does not appear sensitive to vertical canopy structure. Although meriting further investigation, the relatively broad updraft bases in the profile A case and relatively narrow updraft bases in the remaining cases are consistent with the relative strength of within-canopy turbulence (Figure 5; discussed next). Taken together, the horizontal and vertical motion fields in Figures 3 and 4 depict a circulation that becomes narrower and less intense and that penetrates further into the canopy, as canopy structure evolves from overstory concentrated to understory concentrated. Lastly, note that as with $\overline{U}_{yt}$, the spatial pattern of the $\overline{W}_{yt}$ mean anomaly does not change as fire heat flux is increased, only the magnitude (as in Figure 2).

Before proceeding to analysis of $\overline{E}_{yt}$ (Figure 5), a word of caution is in order regarding terminology. For U, W, and T, the difference in mean values between cases with and without fire heat flux is referred to as the mean

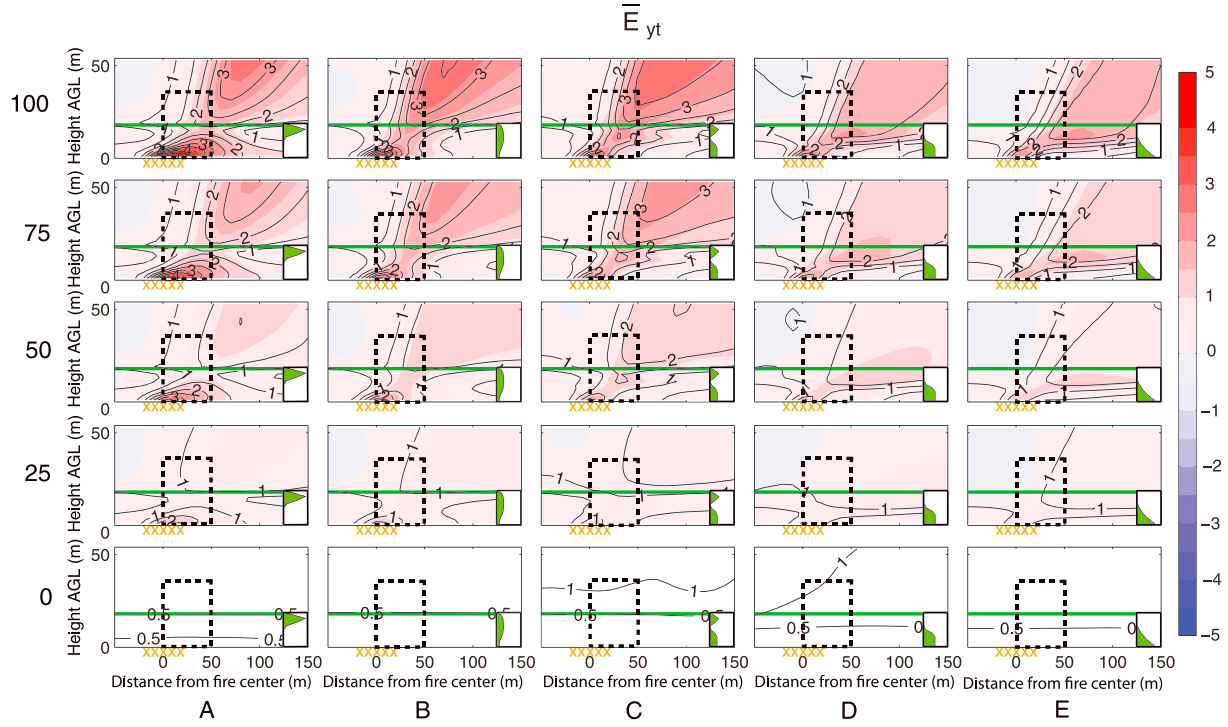

Figure 5. Same as Figure 3 but for E ($\overline{E}_{yt}$; $m^2\ s^{-2}$); interval is 0.5 $m^2\ s^{-2}$ for contours and shading.

anomaly, as it refers to changes in the mean flow due to the fire heat flux. In the context of E, such fire-induced changes are referred to simply as changes (increases or decreases), to minimize confusion, since E computed in the no-fire case contains only turbulent fluctuations, and E computed in the cases with fire heat flux contains both turbulent fluctuations and mean flow anomalies (section 3.1). Recall that our purpose in presenting E is to characterize combined changes to turbulent mixing and mean transport of heat, moisture, and pollutants (e.g., $PM_{2.5}$) due to the sensible heat released from the fire.

Note that in the absence of fire heat flux (Figure 5, fifth row), the atmosphere exhibits both weak mean flow (2.5 m s^{-1} uniform background flow) and weak turbulence ($\overline{E}_{yt}$ values generally at or below 1 $m^2\ s^{-2}$). Mixing and transport potential is therefore low in the absence of fire heat flux. For all vertical canopy structures, introduction of the 25 kW m^{-2} fire heat flux generally yields increased $\overline{E}_{yt}$, with an area of decreased $\overline{E}_{yt}$ upstream of the fireline, above the canopy. The largest increases in surface $\overline{E}_{yt}$ are found with profile A (case A25), with fire-heat-flux-induced changes to $\overline{E}_{yt}$ difficult to distinguish for profiles C–E. The relatively large impact of the fire heat flux on $\overline{E}_{yt}$ in case A25 is explained by the lack of surface vegetation in profile A, with buoyancy-induced E production largely unopposed by canopy drag. This analysis of fire-heat-flux-induced changes to $\overline{E}_{yt}$ suggests an increase in the potential for turbulent mixing and mean transport of heat, moisture, and pollutants due to the sensible heat flux from the fire. Furthermore, the magnitude and spatial pattern of this increase is sensitive to vertical canopy structure. As fire heat flux magnitude is increased from 25 to 100 kW m^{-2}, the influence of vertical canopy structure on fire-heat-flux-induced changes to $\overline{E}_{yt}$ becomes more evident. Beginning with the 50 kW m^{-2} row and moving upward in the matrix, two distinct areas of greater $\overline{E}_{yt}$ increase become evident with overstory-concentrated profile A, with a layer of lesser $\overline{E}_{yt}$ increase near canopy top, in contrast to a more uniform "streak" of $\overline{E}_{yt}$ increase from the fireline through the canopy into the overlying atmosphere downstream of the fireline, with understory-concentrated profiles D and E. The relative minimum in $\overline{E}_{yt}$ change in the upper canopy in the overstory-concentrated cases is the result of canopy drag (and the resultant E sink) in the dense overstory layer.

Proceeding finally to $\overline{T}_{yt}$ (Figure 6), despite daytime near-surface superadiabatic lapse rates (not shown), the use of a relatively large 10°C contour interval results in contour-free panels in the no-fire cases, necessitating comparison of the first to fourth rows only. The presence of a 25 kW m^{-2} fire heat flux yields mainly positive $\overline{T}_{yt}$ mean anomalies, with an area of negative $\overline{T}_{yt}$ mean anomalies upstream of the fireline (likely the result

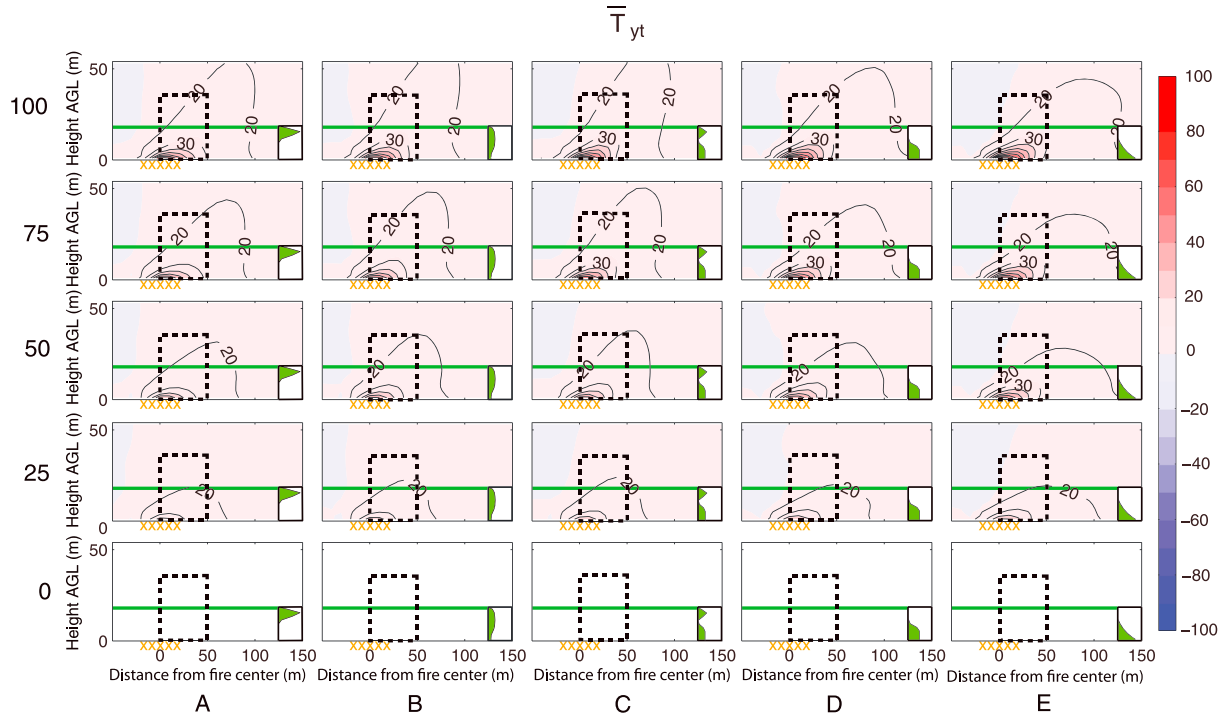

Figure 6. Same as Figure 3 but for T ($\overline{T}_{yt}$; °C); interval is 10°C for contours and shading.

of downward transport of cooler temperatures within the aforementioned downdraft; cf. Figures 4 and 6). Note that negative T mean anomalies have been observed during real-world fires; for example, Heilman et al. (2015) reported such phenomena during a prescribed fire experiment in the New Jersey Pine Barrens (see their Figure 2a). The largest positive mean anomaly is found immediately above the fireline, with an area of enhanced $\overline{T}_{yt}$ extending 50–100 m downstream of the fireline center (as seen in the contoured field). Both the largest $\overline{T}_{yt}$ mean anomaly (32.2°C) and greatest downstream extent of enhanced $\overline{T}_{yt}$ occur with profile E (i.e., case E25), the result of relatively weak turbulent mixing in the near-surface atmosphere (cf. Figures 5 and 6). As fire heat flux magnitude is increased from 25 to 100 kW m^{-2}, the mean anomaly increases in magnitude, reaching as high as 83.4°C in case E100, with the basic pattern of negative and positive $\overline{T}_{yt}$ mean anomalies persisting.

Before proceeding, a few words are in order regarding possible implications of the results outlined in this section. The results presented to this point suggest that perturbation of the atmosphere in and above a forest canopy by sensible heating from a surface fire is sensitive to vertical canopy structure, as evidenced by the $\overline{U}_{yt}$, $\overline{W}_{yt}$, $\overline{E}_{yt}$, and $\overline{T}_{yt}$ cross sections just presented. However, it is worth noting that vertical canopy structure is but one aspect of the forest canopy morphology. Previous work by Kiefer et al. (2016) showed that fire-heat-flux-induced atmospheric perturbations are sensitive to gaps in forest canopies as well as the position of the gaps to the fireline itself, and a study by Kiefer et al. (2015) found notable sensitivity of atmospheric perturbations to PAI, that is, vertically integrated A_p. Thus, it appears that canopy morphology should be accounted for when applying the results of a fire-atmosphere interaction study conducted in one type of forest to other forests with different canopy structures.

3.4. Vertical Profiles

In order to more fully examine vertical gradients of the fire-heat-flux-perturbed variables, the spatiotemporal mean quantities presented in section 3.3 are further averaged in the west-east direction (expressed as $\overline{\Phi}_{xyt}$, where "x" refers to averaging in the x direction). Given the potential applications of a study of fire-heat-flux-perturbed flow in and above a forest canopy (e.g., fire spread and tree mortality), and in the interest of preserving positive and negative perturbations during the averaging procedure, the averaging zone is limited to a 50 m wide zone centered on the downstream edge of the fireline and extending vertically to twice the canopy height (see Figures 3–6 for a depiction of the averaging zone). Furthermore, given the weak

vertical gradients of W (Figure 4), and the apparent insensitivity of the vertical gradients of T to canopy structure (Figure 6), analysis of vertical profiles is limited to U and E ($\overline{U}_{xyt}$ and $\overline{E}_{xyt}$, respectively).

The vertical profile analysis begins with $\overline{U}_{xyt}$ (Figure 7). In the absence of fire heat flux (0 kW m^{-2} row), two distinct classes of vertical $\overline{U}_{xyt}$ profile are seen: one class with a layer of maximum vertical wind shear at the top of the canopy (canopy profiles A–C) and a second class with a layer of maximum vertical wind shear located in the middle of the canopy (canopy profiles D and E). The height of the vertical wind shear maximum is closely linked to the height AGL of the uppermost layer of strong A_p gradient (compare fifth to sixth rows of Figure 7). Note that the overall magnitude of vertical wind shear varies little between canopy profiles A–C, despite considerable differences in the density of overstory vegetation. Finally, note that this evolution is broadly consistent with that shown in Hoffman et al. (2015), wherein the mean wind profile upwind of the fire transitioned from one typical of forested environments, with weak winds in the lowest two thirds of the canopy and maximum vertical wind shear at and just below canopy top, to a log wind profile more typical of nonforested environments, with maximum wind shear near the surface.

Introduction of the 25 kW m^{-2} fire heat flux yields greater sensitivity of the vertical $\overline{U}_{xyt}$ profiles to vertical canopy structure. Specifically, a smooth transition is evident from an "inverse S"-shaped wind profile, with wind speed strongest at the surface and above the canopy and minimized in the upper canopy, in case A25, to a linearly increasing wind profile with minimum wind speed at the surface, in case E25. Comparing the vertical cross sections and profiles of $\overline{U}$ (Figures 3 and 7, respectively), one can see that as the vertical canopy structure transitions from overstory concentrated (profile A) to understory concentrated (profile E), the gradual weakening of the westerly inflow above the fireline (i.e., positive mean anomaly) and the increasing presence of the aforementioned easterly inflow (i.e., negative mean anomaly) in the averaging zone (Figure 3) serve to yield steadily weaker near-surface mean anomalies in the vertical $\overline{U}_{xyt}$ profiles (red bars in Figure 7). Introduction of progressively larger fire heat fluxes amplifies the differences between overstory- and understory-concentrated canopy profiles. A layer of negative wind shear (i.e., wind speed decreasing with height) inside the canopy is evident in the cases with canopy profile A, with positive wind shear (i.e., wind speed increasing with height) within the same layer in the cases with canopy profile E. The negative wind shear layer has been observed and simulated in the absence of fire within the trunk space of forests with dense overstory vegetation and deep, sparse trunk spaces, and this secondary shear layer has been cited as a source of turbulence inside the trunk space of deep canopies (Dupont et al., 2011). It is worth noting that observational (e.g., Clements et al., 2007) and modeling (e.g., Kochanski et al., 2013) studies of grassfires have revealed similar negative shear layers.

We next examine vertical profiles of $\overline{E}_{xyt}$ (Figure 8), and note that in the absence of fire heat flux (0 kW m^{-2} row), mean E is less than 1 m^2 s^{-2} (note that in the absence of fire heat flux, the E presented here is entirely TKE). A transition in the shape of the $\overline{E}_{xyt}$ profile is noted as vertical canopy structure shifts from overstory dominated (canopy profile A) to understory dominated (canopy profile E), with in-canopy $\overline{E}_{xyt}$ maximized at the surface in the former and overstory in the latter. Addition of the fire heat flux amplifies the sensitivity of $\overline{E}_{xyt}$ to vertical canopy structure, with increases in $\overline{E}_{xyt}$ due to the fire heat flux (i.e., red bars) overall largest with canopy profile A and smallest with canopy profile E. Overall, $\overline{E}_{xyt}$ is largest in case A100, with a value of about 5 m^2 s^{-2}, a more than fivefold increase in $\overline{E}_{xyt}$ over the background state. Furthermore, the layer influenced by the fire heat flux is also sensitive to vertical canopy structure, with $\overline{E}_{xyt}$ increases maximized near the surface but extending through the 36 m deep layer with canopy profiles A and B, approximately equally distributed through the layer with canopy profile C, and almost entirely limited to below canopy top with canopy profile E. Note that the limited averaging area utilized in the construction of Figure 8 should be kept in mind when comparing the vertical cross sections of $\overline{E}_{yt}$ in Figure 5 and the vertical profiles of $\overline{E}_{xyt}$ in Figure 8 (see dashed box in Figure 5). Finally, consistent with the vertical cross sections of $\overline{E}_{yt}$ depicted in Figure 5, Figure 8 suggests that the sensible heat flux from the fire increases the potential for turbulent mixing and mean transport of heat, moisture, and pollutants, and the pattern and magnitude of this transformation are sensitive to vertical canopy structure.

3.5. Summary Statistic Line Plots

With analysis of fire-heat-flux-perturbed variables in one- and two-dimensional analyses complete, we now wish to address the question of how the sensitivity of the atmosphere to increases in fire heat flux is affected by vertical canopy structure. In this section, three statistical metrics are examined that describe the fire-heat-flux-perturbed atmosphere within the portion of the domain surrounding the fire: the 10th

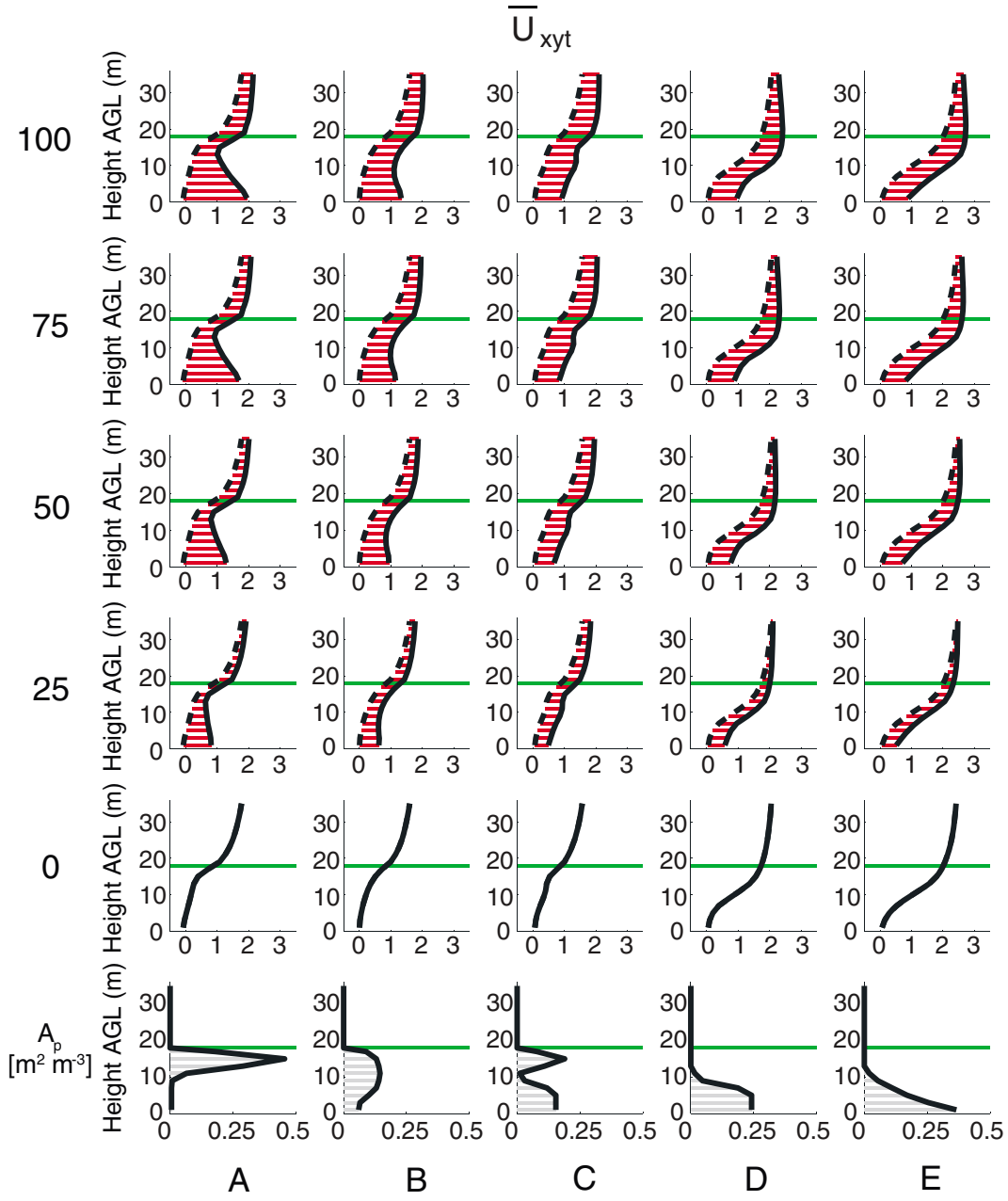

Figure 7. Vertical profiles of U, averaged in time and space as in Figure 3, but further averaged in the x direction ($\overline{U}_{xyt}$; m s^{-1}); see Figure 3 for depiction of averaging zone. The cases are arranged in a 5 × 5 matrix as in Figure 3, with an additional row of panels depicting vertical profiles of A_p included below the matrix. In each panel of the 5 × 5 matrix, the solid black line corresponds to values in that particular case and the dashed black line corresponds to values in the no-fire (i.e., 0 kW m^{-2}) case; at each vertical level in the profile, a red horizontal bar indicates an increase in the variable over the no-fire value (i.e., positive mean anomaly). The green horizontal line in each panel depicts the top of the canopy.

percentile, the median, and the 90th percentile (Figure 9). The statistical metrics are computed using all grid points in the vertical cross sections presented in Figures 3–6 (inside as well as outside of the averaging zone utilized for the vertical profiles). Figure 9 consists of a series of lines connecting the values of each metric for cases with the same vertical canopy structure, but with different fire heat fluxes. For each metric, five colored lines are plotted, corresponding to the five vertical canopy structures examined in this study (canopy profile A: red; B: orange; C: green; D: teal; E: blue). Thus, the slope of each line indicates changes to the metric with vertical canopy structure fixed, and fire heat flux varied, and the horizontal spacing between colored symbols

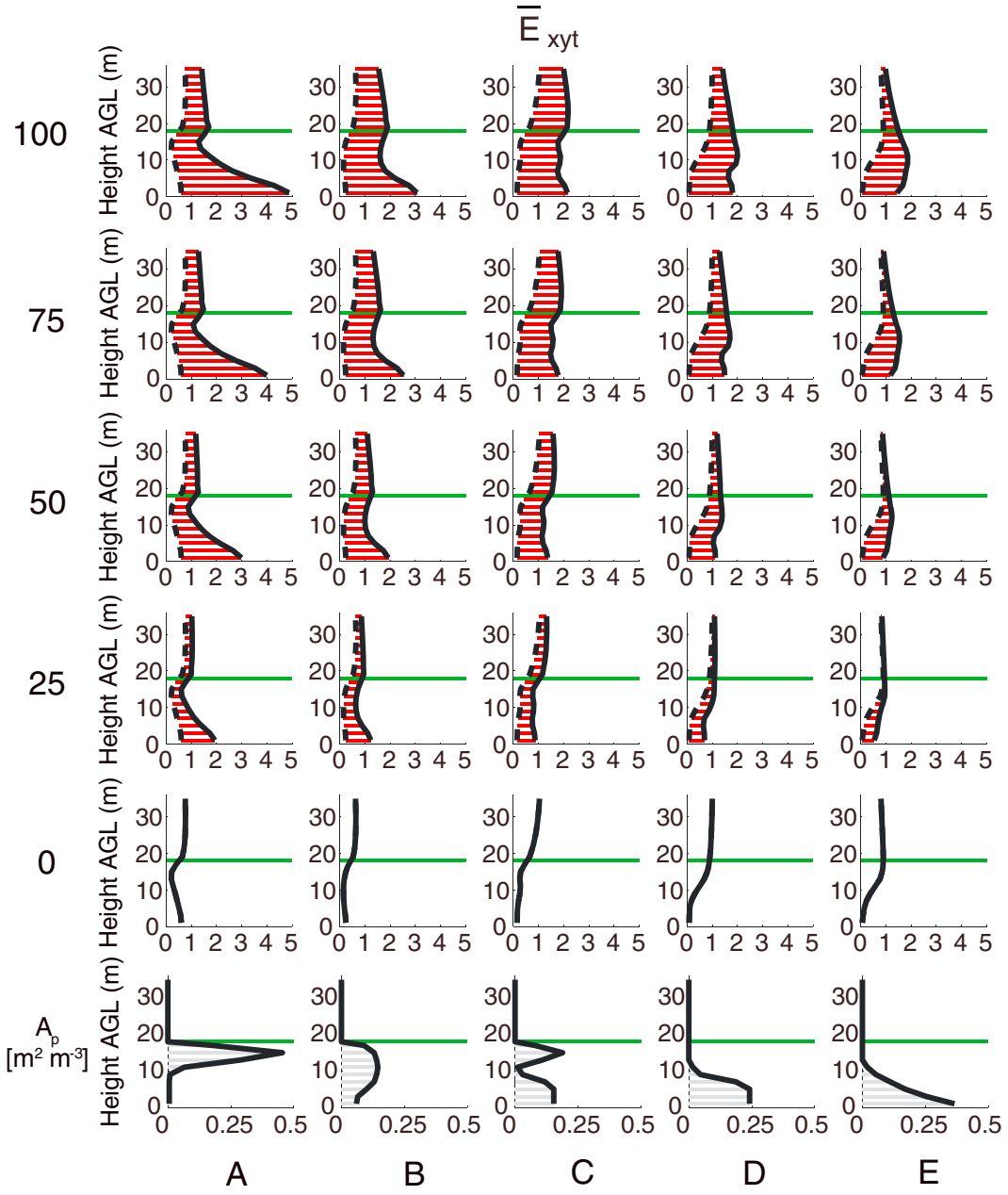

Figure 8. Same as Figure 7 but for E ($\overline{E}_{xyt}$; m^2 s^{-2}).

indicates changes to the metric with fire heat flux fixed, and vertical canopy structure varied. Note that the three metrics were chosen because we are interested in the impact of the sensible heat released by the fire across the broader area surrounding the fireline (e.g., several canopy heights away; represented by the median) as well as in a more localized sense (e.g., immediately above the fireline, at the top of the canopy; represented by the 10th and 90th percentiles).

As a first step, consider the no-fire (0 kW m^{-2}) cases for all four variables (points along the bottom of each panel). Beginning with $\overline{U}_{yt}$ (Figure 9a), similar median and 90th percentile values are seen for canopy profiles A, B, and C (red, orange, and green lines), with notably higher values for canopy profiles D and E (teal and blue lines). The stronger wind speeds with canopy profiles D and E can be attributed to the lack of overstory vegetation, allowing stronger westerly flow to penetrate into the canopy from above (greater number of points with positive $\overline{U}_{yt}$), and the aforementioned shallow depth of the easterly inflow layer (and thus limited

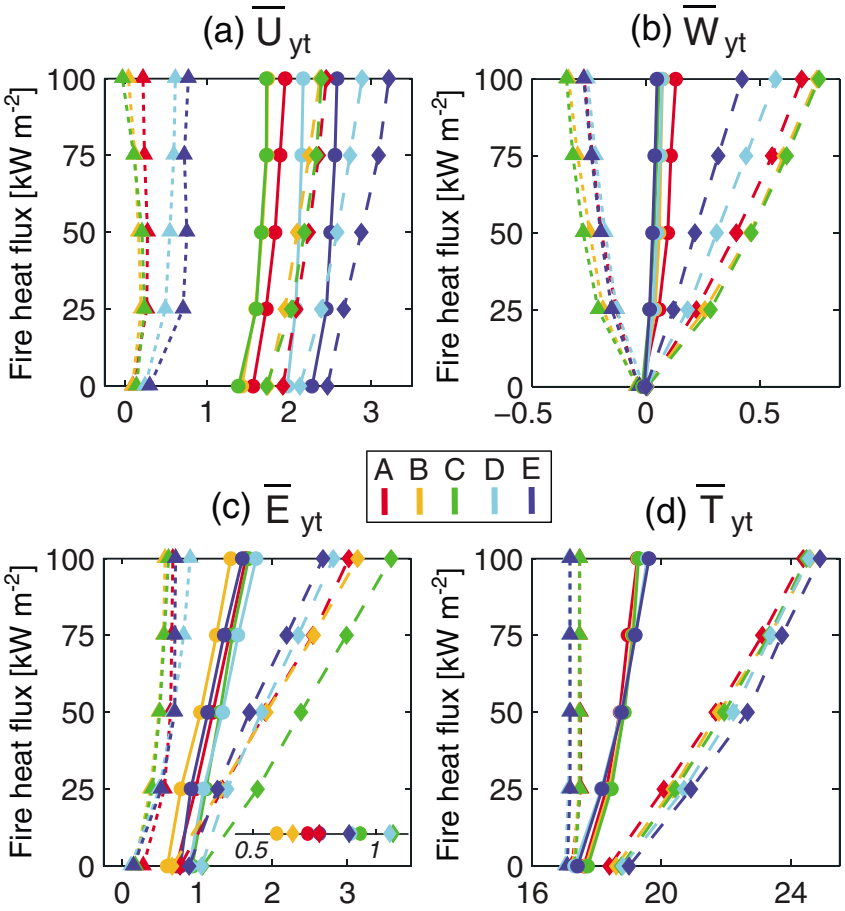

Figure 9. Line plots of the 10th percentile (short dashed line; triangle), median (solid line; circle), and 90th percentile (long dashed line; diamond) values of (a) $\overline{U}_{yt}$ (m s^{-1}), (b) $\overline{W}_{yt}$ (m s^{-1}), (c) $\overline{E}_{yt}$ (m^2 s^{-2}), and (d) $\overline{T}_{yt}$ (°C). In each panel, fire heat flux (kW m^{-2}) varies on the *y* axis, and vertical canopy structure is indicated by color; see legend for the relationship of line color to canopy profile. The inset panel in (c) depicts the median and 90th percentile values for the 0 kW m^{-2} (no-fire) row, zoomed in for clarity.

number of points with negative $\overline{U}_{yt}$). Ignoring for the moment the $\overline{W}_{yt}$ panel (Figure 9b), owing to the very weak nature of vertical motion in the absence of fire heat flux, examination of $\overline{E}_{yt}$ (Figure 9c) shows generally smaller median and 90th percentile values for canopy profiles A and B (red and orange lines), and slightly larger values for canopy profiles C, D, and E (green, teal, and blue lines). The somewhat higher $\overline{E}_{yt}$ values for canopy profiles C, D, and E are likely due to the absence of dense overstory vegetation, allowing for marginally stronger turbulence above the canopy to penetrate further toward the surface than for canopy profiles A or B. Lastly, regarding $\overline{T}_{yt}$ (Figure 9d), median values differ only slightly between cases, and the 90th percentile values increase modestly as vertical canopy structure is varied from overstory dominated (canopy profile A; red line) to understory dominated (canopy profile E; blue line).

Proceeding to analysis of the remaining cases in Figure 9, we pivot back to one of the motivating questions of this study: Although the fire-heat-flux-induced atmospheric perturbations are expected to increase in magnitude with increasing heat flux, is the increasing trend sensitive to vertical canopy structure? To help address this question, we now compare the slope of the 90th percentile lines among cases with different A_p profiles (recall that the slope of the line indicates the change of the metric with vertical canopy structure fixed, but with increasing fire heat flux). Note that we examine the 90th percentiles rather than the outliers, since outliers may represent as few as one or two grid points and thus be unrepresentative of the atmospheric response as a whole. Examining the 90th percentile lines for all four variables, negligible slope differences are found in the $\overline{U}_{yt}$ (Figure 9a) and $\overline{T}_{yt}$ (Figure 9d) panels, but noticeable differences are apparent in the $\overline{W}_{yt}$ (Figure 9b) and $\overline{E}_{yt}$ (Figure 9c) panels. For both $\overline{W}_{yt}$ and $\overline{E}_{yt}$, the increasing trend with increasing fire heat flux is stronger for

the cases with some degree of overstory vegetation (canopy profiles A, B, and C; red, orange, and green lines) than for cases with exclusively understory vegetation (canopy profiles D and E; teal and blue lines) [for $\overline{W}_{yt}$, 0.2 m s^{-1} versus 0.1 m s^{-1} per 25 kW m^{-2} increase, respectively; and for $\overline{E}_{yt}$, 0.6 m^2 s^{-2} versus 0.4 m^2 s^{-2} per 25 kW m^{-2} increase, respectively]. The differences in trends between overstory- and understory-concentrated canopy profiles suggest a damping of the atmospheric response to the sensible heat released by a surface fire when vegetation is most concentrated near the surface.

4. Summary and Conclusions

In this study, ARPS-CANOPY has been utilized in a series of numerical experiments designed to address the question of how vertical canopy structure, as inferred from vertical profiles of A_p, influences the atmospheric response to the sensible heat released by a low-intensity surface fire. To this end, experiments with a spatially and temporally invariant surface sensible heat flux (25 kW m^{-2} magnitude) were conducted with vertical canopy structure varying from overstory concentrated (i.e., exclusively crown vegetation) to understory concentrated (i.e., exclusively surface vegetation), using five A_p profiles exhibiting different shapes but identical PAI. Furthermore, in addition to examining the broader question of the influence of vertical canopy structure on the atmospheric response, the question of whether trends in the magnitude of fire-heat-flux-induced atmospheric perturbations with increasing fire heat flux magnitude are sensitive to vertical canopy structure was also considered. Thus, fire heat flux was varied independently of vertical canopy structure, from 0 to 100 kW m^{-2}, every 25 kW m^{-2}, yielding a total of 25 cases (five A_p profiles and five fire heat fluxes). In analyzing the simulations, a telescoping approach was utilized in which variables were examined in near-surface horizontal cross sections first, west-east oriented vertical cross sections second, west-east averaged vertical profiles third, and summary statistic line plots last.

After examining the flow across the fireline via horizontal cross sections of temporally averaged wind speed, the influence of vertical canopy structure on the atmospheric response to the fire heat flux was explored via vertical cross sections and vertical profiles of the *u* component of the wind, vertical velocity, kinetic energy, and temperature. Analysis of the vertical cross sections largely focused on mean anomalies, that is, fire-heat-flux-induced changes to the mean variables, and analysis of the vertical profiles largely focused on the influence of the fire heat flux on vertical gradients of the mean variables. Beginning with the analysis of vertical cross sections of atmospheric variables, averaged along the fireline and during the time period the fire was engaged, sensitivity of the pattern and magnitude of mean anomalies to vertical canopy structure was noted, with little change to the pattern with increasing fire heat flux. Regarding the *u* component of the wind, vertical canopy structure was shown to impact the magnitude of the positive mean anomaly [larger (smaller) mean anomalies for overstory- (understory-) concentrated canopies] and, in particular, the vertical depth of the negative mean anomaly layer downstream of the fire. The depth of the negative mean anomaly layer was shown to be approximately proportional to the height above the ground of maximum A_p (smallest depth for understory-concentrated vertical canopy structures). Furthermore, as the canopy structure was varied from most overstory concentrated to most understory concentrated, (i) the cores of fire-heat-flux-induced updrafts and downdrafts descended from above to below canopy top, while becoming weaker and more concentrated, (ii) the fire-heat-flux-induced increase in kinetic energy at the surface became weaker in magnitude and less detached from the area of fire-heat-flux-induced kinetic energy increase above the canopy, and (iii) the temperature mean anomalies became larger and the downstream extent of fire-enhanced temperatures became greater.

Examination of vertical profiles, constructed with additional west-east averaging of the variables in the vicinity of the downstream fireline edge, further revealed the impact of vertical canopy structure and fire heat flux on vertical gradients of the *u* component of the wind and kinetic energy. In the absence of fire, sensitivity of the wind profile to vertical canopy structure was limited to the height of the layer of maximum wind shear; however, introduction of the fire yielded differences in both the overall shape of the wind profile and the sign of vertical wind shear inside the canopy, between cases with different canopy profiles. As the vertical canopy structure was varied from overstory to understory concentrated, a transition in the shape of the wind profile was noted, from an "inverse S"-shaped wind profile to a linearly increasing wind profile. Notably, a layer of negative wind shear (i.e., wind speed decreasing with height) was found inside the canopy in cases with predominately overstory vegetation, with positive wind shear (i.e., wind speed increasing with height) found within the same layer in cases with predominately understory vegetation. Furthermore, a gradual transition

in the shape of the kinetic energy profile was noted as the vertical canopy structure shifted from overstory concentrated to understory concentrated, with in-canopy kinetic energy maximized at the surface in the former and overstory in the latter.

The second question of how trends in the magnitude of fire-heat-flux-induced atmospheric perturbations with increasing fire heat flux are impacted by vertical canopy structure was answered mainly via analysis of line plots of the median and 10th and 90th percentile values in each of the cases. The line plots, constructed using all grid points in the vertical cross sections, showed little sensitivity of trends to vertical canopy structure for the *u* component of the wind and temperature, but notable sensitivity for vertical velocity and kinetic energy. For both vertical velocity and kinetic energy, the increasing trend with increasing fire heat flux was stronger for the cases with some degree of overstory vegetation (profiles A–C) than the cases with exclusively understory vegetation (profiles D and E). The differences in trends between overstory- and understory-concentrated canopies suggests a damping of the atmospheric response to the sensible heat released by a surface fire when vegetation is most concentrated near the surface. Note that it is unclear how the differences in atmospheric perturbations between cases revealed in this study might translate to differences in aspects of wildland fires like fire behavior and tree mortality; exploration of potential impacts is left to future work.

More generally, the results presented in this study suggest that canopy morphology should be accounted for when applying the results of a fire-atmosphere interaction study conducted in one type of forest to other forests with different canopy structures. Perturbation of the atmosphere by the sensible heat released from a surface fire, both in terms of pattern and magnitude, is sensitive to the vertical canopy structure. However, the idealized nature of this study must be emphasized. The only interaction represented in ARPS-CANOPY is the perturbation of the atmosphere due to sensible heat flux from the fire. The use of a spatially and temporally invariant surface heat flux neglects the complex interplay between fire, fuels, and atmosphere that occurs in wildland fires. Thus, the results of this study are most directly applicable to low-intensity, slow-spreading surface fires in horizontally homogeneous fuels; in situations that deviate from such conditions, the relationships between sensible heat flux, vertical canopy structure, and atmospheric perturbations revealed in this study may be overwhelmed by other processes. Furthermore, since latent heat release from the fire is neglected in this study, the impact of the fire on buoyancy is likely underestimated compared to real-world fires. Lastly, the use of 10 m wide grid cells precludes the simulation of microscale phenomena like fireline vortices and ejection/sweep events in the forest canopy that can further complicate conditions at the fireline.

Despite the progress documented herein, much work remains. Future efforts planned include implementing a moving fire, accounting for the impact of spatial heterogeneity of forest canopy vegetation on fire heat flux, and examining potential impacts of moisture production from combustion and fuels drying on these and previous ARPS-CANOPY findings. Furthermore, given the aforementioned potential application of the results of this study to studies of tree mortality, future work will also include analysis of fire-heat-flux-perturbed atmospheric variables restricted to the canopy layer only.

Acknowledgments
Support for this research was provided by the USDA Forest Service via Research Joint Venture Agreements 13-JV-11242306-055 and 11-JV-11242306-058. This work was supported partially by the USDA National Institute of Food and Agriculture, Hatch project 1010691. We would like to acknowledge high-performance computing support from Yellowstone (ark:/85065/d7wd3xhc) provided by NCAR's Computational and Information Systems Laboratory, sponsored by the National Science Foundation. We wish to thank three anonymous reviewers for providing helpful comments and suggestions to improve the manuscript. Data from this study are freely available for download at http://eams2.usfs.msu.edu/Pub_Data/outgoing/kiefer/canshape18.

References

Chou, M.-D. (1990). Parameterization for the absorption of solar radiation by O_2 and CO_2 with application to climate studies. *Journal of Climate*, *3*, 209–217.

Chou, M.-D. (1992). A solar radiation model for climate studies. *Journal of the Atmospheric Sciences*, *49*, 762–772.

Chou, M.-D., & Suarez, M. J. (1994). An efficient thermal infrared radiation parameterization for use in general circulation models (Tech. Rep. Tech. Memo 104606). NASA [Available from NASA Center for Aerospace Information, 800 Elkridge Landing Road, Linthicum Heights, MD 21090-2934].

Clark, T. L., Coen, J., & Latham, D. (2004). Description of a coupled atmosphere-fire model. *International Journal of Wildland Fire*, *13*, 49–63.

Clark, T. L., Radke, L., Coen, J., & Middleton, D. (1999). Analysis of small-scale convective dynamics in a crown fire using infrared video camera imagery. *Journal of Applied Meteorology*, *38*, 1401–1420.

Clements, C. B., Zhong, S., Goodrick, S., Li, J., Potter, B. E., Bian, X., et al. (2007). Observing the dynamics of wildland grass fires: FireFlux—A field validation experiment. *Bulletin of the American Meteorological Society*, *88*, 1369–1382.

Dahl, N., Xue, H., Hu, X., & Xue, M. (2015). Coupled fire–atmosphere modeling of wildland fire spread using DEVS-FIRE and ARPS. *Natural Hazards*, *77*, 1013–1035.

Deardorff, J. W. (1980). Stratocumulus-capped mixed layers derived from a three-dimensional model. *Boundary-Layer Meteorology*, *18*, 495–527.

Dupont, S., Bonnefond, J.-M., Irvine, M. R., Lamaud, E., & Brunet, Y. (2011). Long-distance edge effects in a pine forest with a deep and sparse trunk space: In-situ and numerical experiments. *Agricultural and Forest Meteorology*, *151*, 328–344.

Dupont, S., & Brunet, Y. (2008). Influence of foliar density profile on canopy flow: A large-eddy simulation study. *Agricultural and Forest Meteorology*, *148*, 976–990.

Finnigan, J. J. (2000). Turbulence in plant canopies. *Annual Review of Fluid Mechanics*, *32*, 519–571.

Heilman, W. E., Clements, C. B., Seto, D., Bian, X., Clark, K. L., Skowronski, N. S., & Hom, J. L. (2015). Observations of fire-induced turbulence regimes during low-intensity wildland fires in forested environments: Implications for smoke dispersion. *Atmospheric Science Letters*, *16*, 453–460. https://doi.org/10.1002/asl.581

Hiers, J. K., Ottmar, R., Butler, B. W., Clements, C., Vihnanek, R., Dickinson, M. B., & O'Brien, J. (2009). An overview of the prescribed fire combustion and atmospheric dynamics research experiment (Rx-CADRE). In S. Rideout-Hanzak (Ed.), *4th International Fire Ecology and Management Congress: Fire as a global process*. Savannah, Georgia: Association for Fire Ecology.

Hoffman, C. M., Linn, R., Parsons, R., Sieg, C., & Winterkamp, J. (2015). Modeling spatial and temporal dynamics of wind flow and potential fire behavior following a mountain pine beetle outbreak in a lodgepole pine forest. *Agricultural and Forest Meteorology*, *204*, 79–93.

Jenkins, M. A., Clark, T., & Coen, J. (2001). Coupling atmospheric and fire models. In M. A. Jenkins, T. Clark, & J. Coen (Eds.), *Forest fire: Behavior and ecological effects* (pp. 257–302). Cambridge, MA: Academic Press.

Kiefer, M. T., Heilman, W. E., Zhong, S., Charney, J. J., & Bian, X. (2015). Mean and turbulent flow downstream of a low-intensity fire: Influence of canopy and background atmospheric conditions. *Journal of Applied Meteorology and Climatology*, *54*, 42–57.

Kiefer, M. T., Heilman, W. E., Zhong, S., Charney, J. J., & Bian, X. (2016). A study of the influence of forest gaps on fire-atmosphere interactions. *Atmospheric Chemistry and Physics*, *16*, 8499–8509.

Kiefer, M. T., Heilman, W. E., Zhong, S., Charney, J. J., Bian, X., Skowronski, N. S., et al. (2014). Multiscale simulation of a prescribed fire event in the New Jersey Pine Barrens using ARPS-CANOPY. *Journal of Applied Meteorology and Climatology*, *53*, 793–812.

Kiefer, M. T., Parker, M. D., & Charney, J. J. (2009). Regimes of dry convection above wildfires: Idealized numerical simulations and dimensional analysis. *Journal of the Atmospheric Sciences*, *66*, 806–836.

Kiefer, M. T., & Zhong, S. (2015). The role of forest cover and valley geometry in cold-air pool evolution. *Journal of Geophysical Research: Atmospheres*, *120*, 8693–8711. https://doi.org/10.1002/2014JD022998

Kiefer, M. T., Zhong, S., Heilman, W. E., Charney, J. J., & Bian, X. (2013). Evaluation of an ARPS-based canopy flow modeling system for use in future operational smoke prediction efforts. *Journal of Geophysical Research: Atmospheres*, *118*, 6175–6188. https://doi.org/10.1002/jgrd.50491

Kochanski, A. K., Jenkins, M. A., Mandel, J., Beezley, J. D., Clements, C. B., & Krueger, S. (2013). Evaluation of WRF-SFIRE performance with field observations from the FireFlux experiment. *Geoscientific Model Development*, *6*, 1109–1126.

Kremens, R. L., Dickinson, M. B., & Bova, A. S. (2012). Radiant flux density, energy density and fuel consumption in mixed-oak forest surface fires. *International Journal of Wildland Fire*, *21*, 722–730.

Linn, R. R., & Cunningham, P. (2005). Numerical simulations of grass fires using a coupled atmosphere-fire model: Basic fire behavior and dependence on wind speed. *Journal of Geophysical Research*, *110*, D13107. https://doi.org/10.1029/2004JD005597

Moeng, C.-H. (1984). A large-eddy-simulation model for the study of planetary boundary layer turbulence. *Journal of the Atmospheric Sciences*, *41*, 2052–2062.

Pimont, F., Dupuy, J. L., Linn, R. R., & Dupont, S. (2011). Impacts of tree canopy structure on wind flows and fire propagation simulated with FIRETEC. *Annals of Forest Science*, *68*, 523–530.

Pimont, F., Dupuy, J. L., Linn, R. R., & Dupont, S. (2009). Validation of FIRETEC wind-flows over a canopy and a fuel-break. *International Journal of Wildland Fire*, *18*, 775–790.

Powers, J. G., Klemp, J. B., Skamarock, W. C., Davis, C. A., Dudhia, J., Gill, D. O., et al. (2017). The Weather Research and Forecasting (WRF) model: Overview, system efforts, and future directions. *Bulletin of the American Meteorological Society*, *98*, 1717–1737.

Raupach, M., & Thom, A. (1981). Turbulence in and above plant canopies. *Annual Review of Fluid Mechanics*, *13*, 97–129.

Shaw, R. H., Hartog, D., & Neumann, H. H. (1988). Influence of foliar density and thermal stability on profiles of Reynolds stress and turbulence intensity in a deciduous forest. *Boundary-Layer Meteorology*, *45*, 391–409.

Xue, M., Droegemeier, K. K., & Wong, V. (2000). The Advanced Regional Prediction System (ARPS)—A multi-scale nonhydrostatic atmosphere simulation and prediction model. Part I: Model dynamics and verification. *Meteorology and Atmospheric Physics*, *75*, 463–485.

Xue, M., Droegemeier, K. K., Wong, V., Shapiro, A., Brewster, K., Carr, F., et al. (2001). The Advanced Regional Prediction System (ARPS)—A multi-scale nonhydrostatic atmosphere simulation and prediction tool. Part II: Model physics and applications. *Meteorology and Atmospheric Physics*, *76*, 143–165.